ORIGINAL RESEARCH

Enhancement of bone consolidation using high-frequency pulsed electromagnetic short-waves and titanium implants coated with biomimetic composite embedded into PLA matrix: in vivo evaluation

Daniel Oltean-Dan,[1] Gabriela-Bombonica Dogaru,[2] Maria Tomoaia-Cotisel,[3,4] Dragos Apostu,[1] Alexandru Mester,[5] Horea-Rares-Ciprian Benea,[1] Mihai-Gheorghe Paiusan,[1] Elena-Mihaela Jianu,[6] Aurora Mocanu,[3] Reka Balint,[3] Catalin-Ovidiu Popa,[7] Cristian Berce,[8] Gyorgy-Istvan Bodizs,[9] Alina-Mihaela Toader,[10] Gheorghe Tomoaia[1,4]

[1]Iuliu Hatieganu University of Medicine and Pharmacy, Department of Orthopedics and Traumatology, 400132 Cluj-Napoca, Romania; [2]Iuliu Hatieganu University of Medicine and Pharmacy, Department of Medical Rehabilitation, 400347 Cluj-Napoca, Romania; [3]Babes Bolyai University, Faculty of Chemistry and Chemical Engineering, Department of Chemical Engineering, Research Center of Physical Chemistry, 400028 Cluj-Napoca, Romania; [4]Academy of Romanian Scientists, 050085 Bucharest, Romania; [5]Iuliu Hatieganu University of Medicine and Pharmacy, Department of Oral Rehabilitation, Oral Health and Management, 400012 Cluj-Napoca, Romania; [6]Iuliu Hatieganu University of Medicine and Pharmacy, Department of Histology, 400349 Cluj-Napoca, Romania; [7]Technical University of Cluj-Napoca, Department of Materials Science and Engineering, 400641 Cluj-Napoca, Romania; [8]Iuliu Hatieganu University of Medicine and Pharmacy, Center for Experimental Medicine, 400349 Cluj-Napoca, Romania; [9]Rehabilitation Clinic, 400347 Cluj-Napoca, Romania; [10]Iuliu Hatieganu University of Medicine and Pharmacy, Department of Physiology, 400006 Cluj-Napoca, Romania

Correspondence: Gheorghe Tomoaia
Department of Orthopedics and Traumatology, Iuliu Hatieganu University of Medicine and Pharmacy, 47 Gen Traian Mosoiu Street, Cluj-Napoca 400132, Romania
Tel +407 2771 1177
Email profgtomoaia.umfcluj@yahoo.com

Maria Tomoaia-Cotisel
Department of Chemical Engineering, Faculty of Chemistry and Chemical Engineering, Research Center of Physical Chemistry, Babes Bolyai University, 11 Arany Janos Street, Cluj-Napoca 400028, Romania
Tel +402 6459 3833
Email mcotisel.chem.ubbcluj.ro@gmail.com

Purpose: Bone consolidation after severe trauma is the most challenging task in orthopedic surgery. This study aimed to develop biomimetic composite for coating Ti implants. Afterwards, these implants were tested in vivo to assess bone consolidation in the absence or the presence of high-frequency pulsed electromagnetic short-waves (HF-PESW).

Materials: Biomimetic coating was successfully developed using multi-substituted hydroxyapatite (ms-HAP) functionalized with collagen (ms-HAP/COL), embedded into poly-lactic acid (PLA) matrix (ms-HAP/COL@PLA), and subsequently covered with self-assembled COL layer (ms-HAP/COL@PLA/COL, named HAPc).

Methods: For in vivo evaluation, 32 Wistar albino rats were used in four groups: control group (CG) with Ti implant; PESW group with Ti implant+HF-PESW; HAPc group with Ti implant coated with HAPc; HAPc+PESW group with Ti implant coated with HAPc+HF-PESW. Left femoral diaphysis was fractured and fixed intramedullary. From the first post-operative day, PESW and HAPc+PESW groups underwent HF-PESW stimulation for 14 consecutive days. Biomimetic coating was characterized by XRD, HR-TEM, SEM, EDX and AFM.

Results: Osteogenic markers (ALP and osteocalcin) and micro-computed tomography (CT) analysis (especially bone volume/tissue volume ratio results) indicated at 2 weeks the following group order: HAPc+PESW>HAPc≈PESW (P>0.05) and HAPc+PESW>control (P<0.05), indicating the higher values in HAPc+PESW group compared to CG. The fracture-site bone strength showed, at 2 weeks, the highest average value in HAPc+PESW group. Moreover, histological analysis revealed the most abundant COL fibers assembled in dense bundles in HAPc-PESW group. At 8 weeks, micro-CT indicated higher values only in HAPc+PESW group vs CG (P<0.05), and histological results showed a complete-healed fracture in groups: HAPc+PESW, HAPc and PESW, but with more advanced bone remodeling in HAPc+PESW group.

Conclusion: Using Ti implants coated by HAPc jointly with HF-PESW stimulation positively influenced the bone consolidation process, especially in its early phase, thus potentially providing a superior strategy for clinical applications.

Keywords: fracture healing, HF-PESW, titanium implants, biomimetic composite coating, multi-substituted hydroxyapatite, collagen fibers

Introduction

According to data of 2016, in the United States alone, approximately 7.9 million fractures occur annually, and between 5% and 10% of them have either delayed bone consolidation or subsequent nonunion healing.[1]

Regarding bone regeneration, the autologous bone graft remains the gold standard ensuring high osteogenic potential.[2] However, due to the risks and complications associated with their harvesting as well as the limited amount of the autologous bone graft that can be collected,[3] to promote osseointegration and bone consolidation need developing effective alternatives.

In order to facilitate osseointegration of titanium implants,[4–6] there have been proposed coatings, such as hydroxyapatite (HAP), collagen (COL), other extracellular matrix proteins and even autologous osteoblasts, that were suitable to enhance bone healing and regeneration.[7–12] The HAP/COL composites were used on rabbits to demonstrate their ability to heal osteochondral defects,[13] showing active bone tissue formation.[14]

Ionic substitutions within the HAP lattice cause changes in the surface structure and local electrical charge, thus increasing the solubility and the ability of the resulting substituted HAPs to participate efficiently in the natural bone remodeling process.[15] Although the concentration of ions that are partially substituting the HAP lattice is small,[16–20] the major resulting effect of released ions is well known in the bone biochemistry.[21–23]

Poly-lactic acid, PLA, is one of the most attractive bioresorbable polyesters[24] due to its high mechanical properties and non-toxic metabolites.[25] The clinical usage of PLA is limited due to its poor hydrophilicity and difficulty in controlling the rate of hydrolysis.[26] Therefore, the use of HAP@PLA composites can reduce the rate of PLA degradation and reinforce the biomaterials.[27] Experimental studies[28–32] on bone models have shown that these composites have an active role in bone formation at the bone–implant interface by facilitating ossification without causing inflammation.[30]

Up to now, the application of porous PLA coatings mineralized through incorporation of multi (Mg, Zn and Si) substituted hydroxyapatite (ms-HAP), such as HAP-1.5wt% Mg-0.2wt%Zn-0.2%wtSi, as nanoparticles (NPs) coated with collagen (i.e., ms-HAP/COL), and dispersed into the PLA matrix, resulting the ms-HAP/COL@PLA composite, has never been reported for bone fracture healing. Therefore, this study aimed to develop an innovative coating for Ti implants.

Further, the adverse effects of stress shielding caused by the use of metallic implants have led to increased research efforts to develop new composites based on HAP@PLA that match the elastic modulus of human bone. Furthermore, it was determined that composites with HAP content ranging between 70 and 85 wt% in PLA matrix have mechanical properties that match those of human cortical bone.[33]

Therefore, we hypothesized that the use of ms-HAP/COL content between 71 and 76 wt% in PLA matrix can determine the composite coatings to reasonably fulfill natural bone needs. From this perspective, the aim of present work was to prepare and investigate the complex composite made of ms-HAP/COL@PLA, for ms-HAP/COL: PLA weight ratios between 71:29 and 76:24. Subsequently, this composite was covered with a self-assembled COL layer, resulting in ms-HAP/COL@PLA/COL, named HAPc, which is highly biocompatible, multi-functional composite for coating on titanium implants. This quality of multi-functional HAPc composite is supported by the COL ability to enhance the adherence of cells,[12,16] which play an important role in callus formation and fracture healing. Additionally, this multi-functional HAPc composite may have an increased capacity for recruiting cells for the in vivo bone fracture healing. Moreover, HAPc coatings on Ti-surface can adapt themselves to changing physiological conditions surrounding the bone, by releasing essential ions from ms-HAP integrated within coatings.

Among the coating techniques, the chemical deposition using a layer by layer method is the most promising, allowing to obtain multi-layered coatings with well-preserved stoichiometry of ms-HAP, as well as to control the outermost self-assembled COL layer of HAPc coating and its surface roughness. In our previous work,[16] the layer by layer method was confirmed to be suitable for the preparation of combined multi-layered biomaterials using ms-HAP, COL and CHI (chitosan) assembled layers, which were successfully used in the in vitro study.

Regarding the bone consolidation and spinal fusion, pulsed electromagnetic field (PEMF) stimulators are the most commonly used noninvasive methods.[34–36] The PEMF therapy has different characteristics and energy output, so it can stimulate different pathways of bone formation and osteoblastogenesis.[37,38] Conversely, high-frequency pulsed electromagnetic fields were found to stimulate osteogenic differentiation on murine precursor cells.[39] Therefore, the effect of uncoated and biomimetic HAPc coated Ti implants jointly with high-frequency pulsed electromagnetic short-waves (HF-PESW) stimulation was evaluated in vivo in this study for bone consolidation.

Hence, the main objectives of this work were: 1) developing the biomimetic coating; 2) quality testing it; and 3) in vivo testing the biomimetic HAPc composite

coated and uncoated Ti implants both in the absence and in the presence of HF-PESW stimulation.

Experimental section

The flowchart of the performed experiments and analyses is shown in Figure 1.

Materials and sample preparation

In order to prepare the HAPc composite, based on PLA mineralized with ms-HAP/COL, and further covered with an adsorbed layer of self-assembled COL, noted as ms-HAP/COL@PLA/COL, for the coating of titanium rods (implants), the following materials were used: PLA 3051 D, obtained from NatureWorks, Minnetonka, MN, USA; dichloromethane high purity, acetone ≥99.5%, type 1 COL from bovine Achilles tendon lyophilized powder, and an 85% phosphoric acid aqueous solution, 99.99% purity, all purchased from Sigma–Aldrich (St Louis, MO, USA).

Titanium (Ti) rods

Ti rods (99.6% purity) of 1.5 mm diameter and 20 mm long were purchased from Goodfellow Cambridge Limited, Huntingdon, England. In order to provide both an appropriate size and surface roughness, the Ti rods were ground to 1.0 mm diameter with abrasive papers. Then, the Ti rods were cleaned using a high-intensity ultrasonic processor Sonics Vibra-Cell, model VCX 750 (Sonics & Material Inc., Newtown, CT, USA) in deionized water at room temperature for 2 hrs. The surface nano-roughness, namely average value Ra 153±10 nm and calculated root mean square, RMS 184±10 nm, was determined on Ti plates (ground by the same method as the Ti rods) by atomicforce microscope (AFM), for a scanned area of 20 μmx20 μm.

For chemical activation of Ti surface and control of the surface roughness, the Ti rods were immersed vertically in a 50 wt% phosphoric acid solution, for 10 mins. Subsequently, the Ti rods were washed with ultrapure water for 5 times to remove the excess of acid from the metal surface. A nano-roughness (of Ra 198±10 nm and RMS 235±10 nm) was determined for these acid etched Ti implants by AFM, for a scanned area of 20 μmx20 μm. Certainly, phosphoric acid treatment increases the nano-roughness of Ti surface in a controlled manner by using various phosphoric acid concentrations for a different action time. The phosphate ions incorporated into the Ti surface[40] can serve as an anchor for the coating with novel biomimetic HAPc composite. For uses in vivo study, the Ti implants treated with phosphoric acid were named pure (uncoated) Ti implants, and those subsequently coated with biomimetic HAPc composite were called HAPc coated Ti implants.

Preparation of ms-HAP/COL nanomaterial

The ms-HAP/COL lyophilized nano-powder was synthesized by a wet precipitation method as described elsewhere,[16,17] by adjusting the content of cations and anions in ms-HAP (ie, HAP-1.5%Mg-0.2%Zn-0.2%Si)
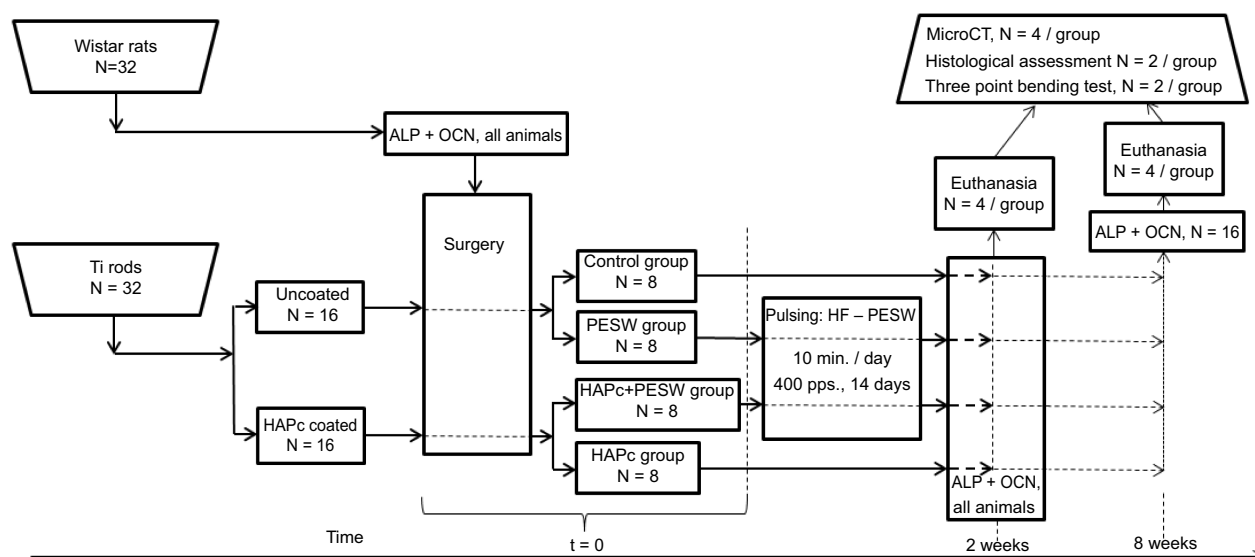

Figure 1 Flowchart of performed experiments and analyses.
Abbreviations: Ti = titanium; HAPc = titanium implant coated with multisubstituted hydroxyapatites and collagen; PESW = pulsed electromagnetic short-waves; HF-PESW = high-frequency pulsed electromagnetic short-waves; ALP = alkaline phosphatase; OCN = osteocalcin; pps = pulses per second.

and the COL content to obtain the chosen ms-HAP:COL (94:6) weight ratio. This ms-HAP was selected, since it has been reported that these elements are well incorporated within HAP lattice, and it has proven a good biological response.[16] The pH of reaction mixture was adjusted to 12, by adding concentrated ammonium hydroxide. All chemicals were purchased from Sigma–Aldrich. The maturation process took place for 24 hrs at 22°C, and ms-HAP/COL NPs were prepared by direct nucleation of ms-HAP nanocrystallites, during the COL self-assembling process. Thus, a new bone-like nanomaterial, ms-HAP/COL, lyophilized powder was prepared, and showed a low crystallinity degree and small crystallite size.

HAPc coating of Ti implants

In order to obtain the HAPc composite for the Ti surface coating, first, a PLA solution was prepared by PLA dissolution in dichloromethane, at room temperature. Then, by adding ms-HAP/COL powder to PLA solution, two dispersions were obtained. Dispersion 1 contains the HAP/COL:PLA, at 76:24 weight ratio, in dichloromethane. Dispersion 1 was diluted with acetone (1:1, v/v) for better flow properties. Dispersion 2 contains ms-HAP/COL:PLA, at 71:29 weight ratio, in dichloromethane.

For HAPc coating of Ti implants, a layer by layer method was used. Briefly, the Ti rods were immersed vertically for three consecutive times in each of the two prepared dispersions, for 30 s each time. The drying time for each adsorbed layer was up to 10 mins at room temperature. Finally, the multi-layered ms-HAP/COL@PLA coating on the Ti implants was covered by a self-assembled COL layer (ms-HAP/COL@PLA/COL, noted as HAPc) obtained by adsorption for 1 min from 1% COL aqueous dispersion, prepared at pH 12 with NaOH. The self-assembly of COL fibers does not imply any external influence but requires slow drying.[41] The surface nano-roughness of HAPc coating on Ti implants, as Ra 505±40 nm and RMS 606±50 nm, was determined by AFM, for 20 μmx20 μm scanned area. All samples were sterilized by ethylene oxide, before animal experiments. The sterilization by dry heat in autoclave was avoided due to the denaturation of COL.

Characterization methods of composites
X-ray diffraction (XRD)

XRD investigations were performed on D8 ADVANCE X-ray diffractometer from Bruker AXS GmbH, Karlsruhe, Germany (Bragg-Brentano geometry) using Cu K_{α} radiation,

wavelength 1.541874 Å, for step-size 0.02 at 2°/min scanning rate. Diffraction patterns were collected in a range of 20–80. A qualitative match procedure was performed with the PDF card number 74-0566 for pure stoichiometric HAP (red lines, in Figure 2A) and with PDF card number 89-4893 for pure Ti (as marked in Figure 2B).

High-resolution-transmission electron microscope (HR-TEM)

HR-TEM images were achieved using FEI Tecnai F20 field emission (FEI Company, Hillsboro, OR, USA), HR-TEM on ms-HAP/COL NPs self-assembled on TEM grids (Figures 2C and D).

Scanning electron microscope (SEM)

SEM images were taken with Hitachi SU-8230 microscope (Hitachi Ltd., Tokyo, Japan), on ms-HAP/COL particles (Figure 2E) deposited on SEM grids. SEM was equipped with Oxford (Oxford Instruments Nanoanalysis, High Wycombe, UK) energy-dispersive X-ray spectrometer (EDS) for elemental analysis, and the energy-dispersive X-ray, EDX, spectrum is given in Figure 2F, for ms-HAP/COL nano-composite. Also, the morphology of biomimetic HAPc composite deposited on Ti (plate) surface, which had the same surface characteristics as Ti (rods) implants, was investigated by SEM (Figures 2G and H).

Atomic force microscope

AFM images were obtained using an AFM JEOL 4210 equipment (JOEL GmbH, Freising, Germany), operated in tapping mode,[29,41,42] using standard cantilevers with silicon nitride tips (resonant frequency in the range of 200–300 kHz, and spring constant 17.5 N/m). The surface roughness of Ti implants (uncovered or covered with HAPc composite) was expressed as the arithmetic mean, Ra, and root mean square, RMS, and was estimated using AFM. Each experiment was repeated 5 times for at least 3 specimens of each experimental group (Figures 2I–L).

Study protocol

The study protocol and all the procedures were approved by the Ethics Committee of "Iuliu Hatieganu" University of Medicine and Pharmacy (UMP), Cluj-Napoca, and eterinary Sanitary Committee (Approval No. 85/19.07.2017). The experimental study was performed according to the principles of the Basel Declaration. Wistar albino rats provided by the Centre of Experimental Medicine of UMP (N=32) were divided equally into the four groups (N=8 in a group): CG (control group) with uncoated, acid etched Ti
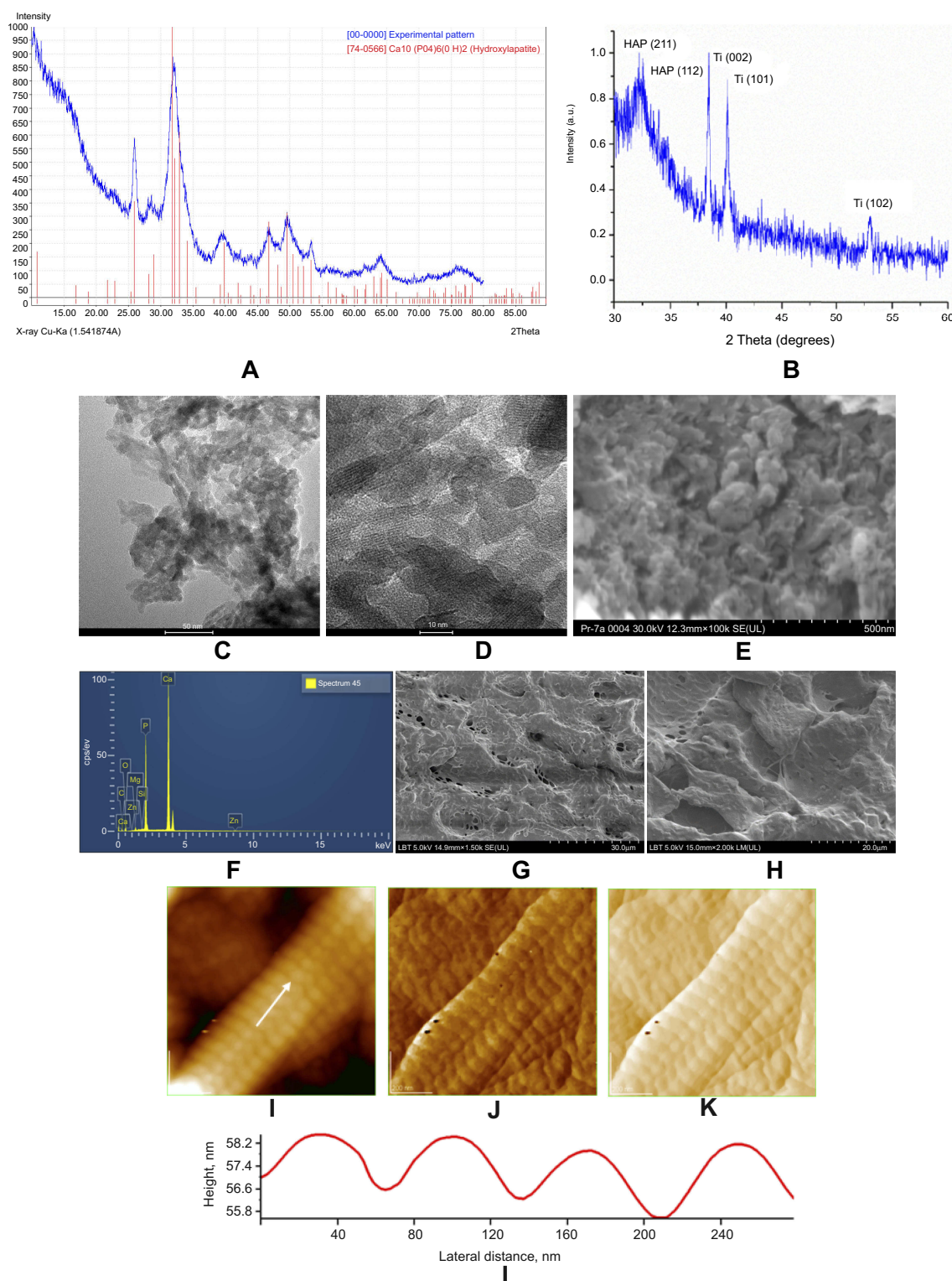
Figure 2 XRD pattern for ms-HAP/COL lyophilized powder (**A**) and for HAPc composite (ie, ms-HAP/COL@PLA/COL) coating on Ti surface (**B**); HR-TEM images (**C, D**) for ms-HAP/COL nanoparticles; SEM image (**E**) and EDX spectrum for same area (**F**) for ms-HAP/COL; SEM images (**G, H**) of the surface of HAPc coating on Ti; AFM images (**I–K**) of a COL fiber self-assembled in the COL layer of HAPc coating on Ti: 2D-topography (**I**), phase image (**J**) and amplitude image (**K**), for scanned area of 1 μm×1 μm; cross-section profile (**L**) on the white arrow in (**I**).

Abbreviations: XRD = X-ray diffraction; ms-HAP/COL = multisubstituted hydroxyapatite/collagen; ms-HAP/COL@PLA/COL = multisubstituted hydroxyapatite/collagen and poly-lactic acid/collagen; Ti = titanium; HAPc = titanium implant coated with multisubstituted hydroxyapatite and collagen; HR-TEM = high resolution transmission electron microscope; SEM = scanning electron microscope; EDX = energy-dispersive X-ray spectometer; AFM = atomic force microscope; COL = collagen.

implants; PESW group with uncoated, acid etched Ti implants and biophysical HF-PESW stimulation; HAPc group with titanium implants coated with HAPc (ie, ms-HAP/COL@PLA/COL); HAPc+PESW group with titanium implants coated with ms-HAP/COL@PLA/COL and HF-PESW stimulation.

Surgical procedures

Surgeries were performed by orthopedic surgeons. The rats were 2 months old and weighed about 226±13 g. They were general anesthetized using a cocktail of xylazine (Bioveta, Cluj-Napoca, Romania; Xylazine Bio 2%) and ketamine hydrochloride (Biotur, Alexandria, Romania; Ketamine 10%), administered intramuscularly. For this surgery technique, a fracture of the middle third left femur was produced by a lateral approach. Intramedullary Ti implants (nails) of 20 mm×1 mm were introduced retrogradely into the medullary canal through the intercondylar femoral notch in rats from CG and PESW group. Titanium implants coated with ms-HAP/COL@PLA/COL were used in HAPc and HAPc+PESW groups. In the end, the subcutaneous layer and the tegument were sutured. Tetracycline unguent was applied on the operative sites. Postoperative, animals were fed ad libitum and housed in cages under controlled environment with 12 hrs light/dark cycle and room temperature of about 22°C.

From the first post-operative day, the rats from the PESW and HAPc+PESW groups were exposed to non-thermal electromagnetic short-waves with a frequency of 400 pulses/s, for 10 min/day, every day, for 2 weeks provided by the Diapulse machine (Diapulse Corporation of America, Great Neck, NY, USA). The mean power was 25.35 W, with a peak power of 975 W, and a total energy of 15.21 kJ.

At 2 weeks post-operative, four rats from each group (N=16, N=4/group) were euthanized using anesthetic overdose. At 8 weeks, the rest of the animals (N=16, N=4/group) were euthanized using the same method. The skin and all the soft tissue from the left thigh were carefully dissected, and then the left femoral bone was harvested. It was cleaned by all the surrounding tissue taking care not to harm or disrupt the bone callus, and then placed in 10% formaldehyde.

Bone markers determination

From retro-orbital sinus, about 0.6 mL of blood was harvested from each rat/examination, before the surgery (N=32), at 14 days (N=32) and at 56 days (N=16). The

samples were centrifuged for 20 mins at 1000xg. After the supernatants were carefully collected, immediately an assay for bone markers was performed. Commercially available ELISA kits were used to measure the concentration of osteocalcin [OCN, Rat OC/BGP (OCN) ELISA kit] and ALP [Rat ALPL ELISA kit]. As detection method for the ALP and OCN values, quantitative sandwich ELISA kits were used.

Histological assessment. Hematoxylin and eosin (H&E) staining

From each of the four groups: CG and PESW, HAPc and HAPc+PESW groups, at 2 weeks (N=2/group) and 8 weeks postoperative (N=2/group), hematoxylin and eosin (H&E) stained tissue samples were analyzed by optical microscopy to assess the evolution of bone callus formation and fracture healing.

Initially, the femurs of rats were fixed in buffered 4% paraformaldehyde for 24 hrs. Decalcification was performed at 4°C under continuous shaking in 5% nitric acid solution. Testing was done using a surgical blade, considered to be completed when the blade easily penetrated the bone without any force. Afterwards the samples were washed in running tap water for 24 hrs and then subjected to dehydration and paraffin embedding. Using a microtome (Leica, Wetzlar, Germany), sections of about 5 μm in thickness were obtained. After deparaffinization and rehydration, the sections were stained with hematoxylin solution for 5 mins followed by 5 dips in 1% HCl in 70% ethanol. Then, the sections were rinsed in distilled water and stained with eosin solution for 3 mins.

Using a Leica DMD 108 optical microscope, the mounted slides were evaluated and photographed. In optical images, chondrocytes, COL fibers, trabeculae of bone and lamellar bone could be observed through a variety of colors, specific for H&E stained tissue, namely COL fibers (pale pink).

Micro-computed tomography

The samples were cleaned with saline solution (0.9%) to remove excess formaldehyde and then were put into the Bruker micro-computed tomography (CT) system SkyScan 1172 for scanning (Bruker microCT, Kontich, Belgium). The region of interest (ROI) was established between the upper and lower limits of the callus, and the total tissue volume (TV), total bone volume (BV) and bone volume relative to total tissue volume (BV/TV)

ratio were determined using the software provided by the system manufacturer. The scan was performed on the long axes of the femoral diaphysis, with a resolution of 16 μm^3 voxel size. Global threshold for analysis was chosen in the range from 225 to 700, which represents the X-ray attenuation between less dense newly formed bone and calcified cartilage (225–330), very dense cortical bone (331–700) and un-mineralized tissue (<225). The same-specific settings and thresholds were applied for each analysis to every sample in the study.

Three points bending test

Afterwards the implants (nails) were extracted carefully, not to induce any crack; then, half of the samples in each group (N=4/group) were evaluated through the three points bending test in order to assess the bone strength in the healed fracture area. The custom-made device used 6 mm diameter steel cylinders for the loading pin and the two supporting pins were placed at a 20 mm distance. The force (F) was applied in the fracture focal point on a Zwick All 5000 (Fmax. 5000 N) testing machine equipped with the TestXpert II software (Zwick Roell, Ulm, Germany), with an accuracy in the measured values range of 0.2%.

Statistical analysis

GraphPad Prism 6 (GraphPad Software, Inc., La Jolla, CA, USA) for Windows was used for statistical analysis. All data are defined as the mean value ± SD of three independent experiments. Significant differences were identified using the two-way ANOVA followed by Tukey post-hoc test. Differences among groups were considered statistically significant if $P<0.05$.

Results
XRD

The XRD pattern of ms-HAP/COL powder (blue) is given in Figure 2A and is characterized primarily by diffraction peaks, at 2θ=31.7 (hkl: 211) which is the most intense peak, and at 32.8° (hkl: 112), corresponding to monophasic ms-HAP NPs coated with COL. The red lines are characteristic of stoichiometric pure HAP [$Ca_{10}(PO_4)_6(OH)_2$], taken from PDF card number 74-0566 and used for comparison with the experimental blue pattern. XRD pattern of the HAPc composite, as a thin layer of ms-HAP/COL@PLA/COL deposited on Ti surface, is given in Figure 2B. One can see the weak diffraction peaks of ms-HAP/COL and more

intense peaks for Ti. This is very consistent with the coexistence of the porous HAPc coating on Ti surface.

Morphology and surface structure

To describe the morphology and surface structure of investigated bio-composites, various techniques were used: HR-TEM images (Figures 2C and D), SEM image (Figure 2E) and EDX spectrum (Figure 2F) for ms-HAP/COL. Further, EDX spectrum (Figure 2F) shows elemental composition of ms-HAP as HAP-1.5%Mg-0.2%Zn-0.2%Si. SEM images of multi-layered HAPc composite deposited on Ti implants are shown in Figures 2G and H. AFM images of self-assembled COL fibers within the outermost layer of the HAPc composite: 2D topography (Figure 2I), phase image (Figure 2J) and amplitude image (Figure 2K), as well as the cross-section profile (Figure 2L) along the arrow in Figure 2I, on the long axis of COL fiber, demonstrate a banding pattern of 67±4 nm, for scanned area of 1 μmx1 μm.

Animal studies

At the end of the experiments, the rats had a weight of 292 ±17 g. There were no deaths or other complications, general or local. All animals regained the normal aspect of their lower limb and had normal gait.

Bone markers concentration

Serum concentrations of bone markers, such as ALP and OCN, are given in Figure 3 at different times. Concentrations of ALP and OCN did not show statistically significant differences ($P>0.05$) among the four groups at the beginning (0 week) and at 8 weeks of the experiment. At 2 weeks, a significant increase of ALP values ($P<0.05$, Figure 3A), was found in each group compared to the initial values. The four groups were in the following order: HAPc +PESW>HAPc=PESW>control. There were significantly lower ALP values ($P<0.05$, Figure 3A) in the CG vs PESW group ($P=0.02$), CG vs HAPc group ($P=0.045$) and CG vs HAPc+PESW group ($P=0.0015$), but no statistically significant differences ($P>0.05$) between groups: HAPc +PESW, HAPc and PESW. Nevertheless, the ALP values in HAPc+PESW group are slightly higher than those in HAPc=PESW groups. The OCN concentrations vs time (Figure 3B) revealed a similar trend as in the case of ALP values (Figure 3A). At 2 weeks, the groups were in the following order: HAPc+PESW>PESW≈HAPc>control. There were significantly lower OCN values in the CG vs PESW group ($P=0.014$), CG vs HAPc group ($P=0.038$) and

CG vs HAPc+PESW group (*P*=0.0002). There was no statistically significant difference (*P*>0.05) between groups: HAPc+PESW, HAPc and PESW.

Micro-computed tomography

Regarding the total TV at 2 weeks (Figure 4A), CG showed lower TV values compared to both groups PESW (*P*=0.02) and HAPc+PESW (*P*=0.005), but without statistical significance (*P*>0.05) between the other groups. The groups were in the following order: HAPc+PESW>PESW>HAPc>control, but the values in HAPc+PESW group are only slightly higher than those in groups HAPc and PESW, which is a similar situation with ALP and OCN data. As shown in Figure 4B, the BV at 2 weeks is significantly lower in CG vs the PESW group (*P*=0.0028), CG vs HAPc group (*P*=0.045) and CG vs HAPc+PESW group (*P*=0.0003) and the tendency among groups is similar with that found in Figure 4A. As shown in Figure 4C, the BV/TV ratio at 2 weeks is significantly lower in the CG compared to both the PESW group (*P*=0.025) and HAPc+PESW group (*P*=0.004). The tendency among groups is similar to that found in Figure 4A and B.

At 8 weeks, the TV substantially decreased (Figure 4A), whereas the BV (Figure 4B) and BV/TV ratio (Figure 4C) significantly increased, in each group compared to the values at 2 weeks. At 8 weeks, the TV for the CG was significantly higher (*P*<0.05, Figure 4A) than the values in the other groups: HAPc+PESW, HAPc or PESW. Figure 4B shows the BV values at 8 weeks; there were no statistically significant differences among the four groups (*P*>0.05). Based on the data in Figure 4C, the groups were in the following order: HAPc+PESW>HAPc=PESW>control, but the BV/TV ratio was significantly higher only in the HAPc+PESW group (*P*<0.05) compared to CG, at 8 weeks, suggesting a potential synergistic effect when both methods are jointly used.

Three points bending tests

The results of the three points bending tests are shown in Figure 5 up to the moment of failure, for periods of 2 and 8 weeks, respectively. The curves generally present an initial stage corresponding to micro-rearrangements of the specimens on the testing device (due to the asymmetric cross-section of the femur), followed by quasi-linear stages showing the elastic character of the deformation. Usually, these are followed by changes in the slope, determined by permanent deformation prior to final failure. This was caused mainly by the occurrence of cracks. The values of ultimate force and the corresponding

displacement for samples implanted for 2 or 8 weeks are shown in Table 1.

Histological analysis

Discussions

Certainly, bone consolidation and fracture union healing after severe trauma are the most challenging tasks in orthopedic surgery. To enhance the bone fracture healing, the coating of Ti implants with bioactive HAPc material, having composition, structure and biological features that mimic the natural healthy bone was a goal in this investigation. The biomimetic HAPc composite was successfully prepared and deeply characterized.

Clearly, the blue diffractogram of ms-HAP/COL lyophilized powder matches the red pattern of HAP structure (Figure 2A), showing that the amount of substituted elements does not significantly affect the crystal lattice of HAP. From XRD analysis, the size of crystallites was about 19 nm and crystallinity degree was around 25%. From the analysis of HR-TEM images (Figures 2C and D), it was found that the ms-HAP/COL is composed of nano-sized needle-like particles, about 20 nm long. SEM image (Figure 2E) shows aggregates of needle-like particles loosely packed, exhibiting a substructure consisting of NPs, in substantial agreement with the HR-TEM and XRD results. The ms-HAP/COL nanomaterial was also evaluated by EDX, Figure 2F, and was found the amount in substituted elements to be close to the chosen composition for ms-HAP, specifically HAP-1.5%Mg-0.2%Zn-0.2%Si. Furthermore, the cations/anions ratio is about 1.68 indicating that this is a stoichiometric ms-HAP. These results showed that the elements were incorporated successfully into HAP lattice.

The XRD pattern of HAPc composite coating [ie, ms-HAP/COL@PLA/COL, noted as HAP-1.5%Mg-0.2%Zn-0.2%Si/COL@PLA/COL] on Ti surface is characterized by three peaks specific for pure Ti, marked in the Figure 2B, and two peaks characteristic for ms-HAP/COL also marked, indicating an amorphous structure of PLA and of self-assembled COL. This finding is characteristic for XRD spectra of thin films deposited on Ti surface.[43]

The morphology of the multi-layered HAPc composite deposited on Ti surface is given in SEM images, Figures 2G and H, indicating a uniform porous structure. It is important to underline that all the components show a good distribution within PLA matrix. There are no large aggregates and, in
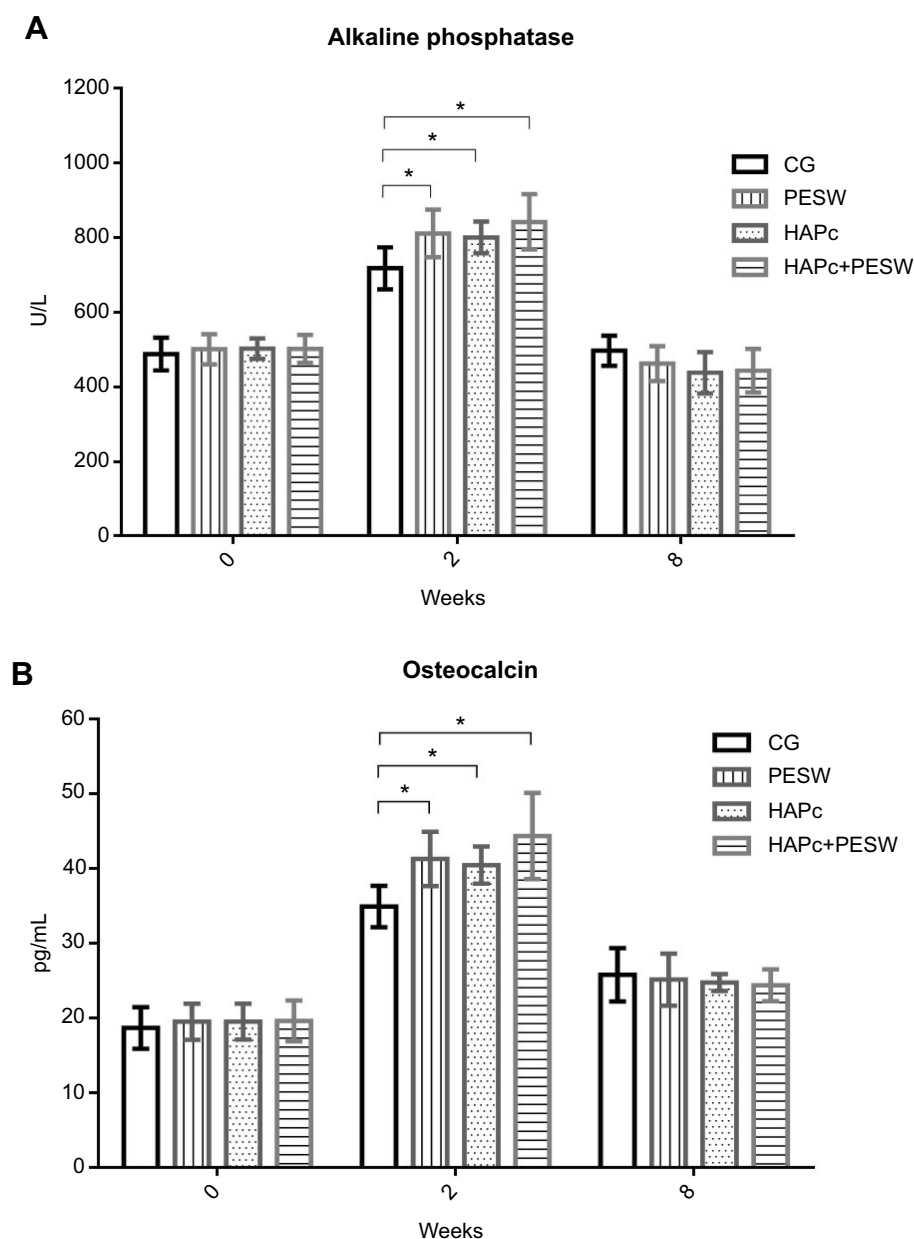
A

B

Figure 3 Serum concentrations of bone formation markers: ALP (U/L, in panel **A**) and OCN (pg/mL, **B**). Error bars stand for SD. Data are given as mean ± SD. Statistically significant differences for P<0.05 are (*) marked.
Abbreviations: CG = control group; PESW = pulsed electromagnetic short-waves; HAPc = titanium implants coated with multisubstituted hydroxyapatite and collagen; HAPc+PESW = titanium implants coated with multisubstituted hydroxyapatite and collagen and pulsed electromagnetic short-waves.

consequence, the ms-HAP/COL particles are also well dispersed in PLA matrix. The self-assembled COL fibers are observed in the surface layer of HAPc coating, particularly at higher magnification, in Figure 2H. The nanostructure of COL fiber was observed in AFM images (Figure 2I–K). The cross-section profile evidences a banding pattern of 67 ±4 nm (Figure 2L), similarly to the native COL fibers.[41] The average thickness of the HAPc coating is about 3.5±0.3 μm, as estimated from the cross-section AFM images.

The present study further evaluates in vivo the bone fracture healing and bone consolidation in the four groups of rats, using Ti implants (uncoated or coated with biomimetic HAPc composite) in the absence or in the presence of HF-PESW stimulation (details are given in Figure 1).

The serum concentrations of bone markers for ALP and OCN are given, in Figure 3, at 0, 2 and 8 weeks. The values at 2 weeks were significantly higher than the initial values at week 0 in all groups, with an increase of
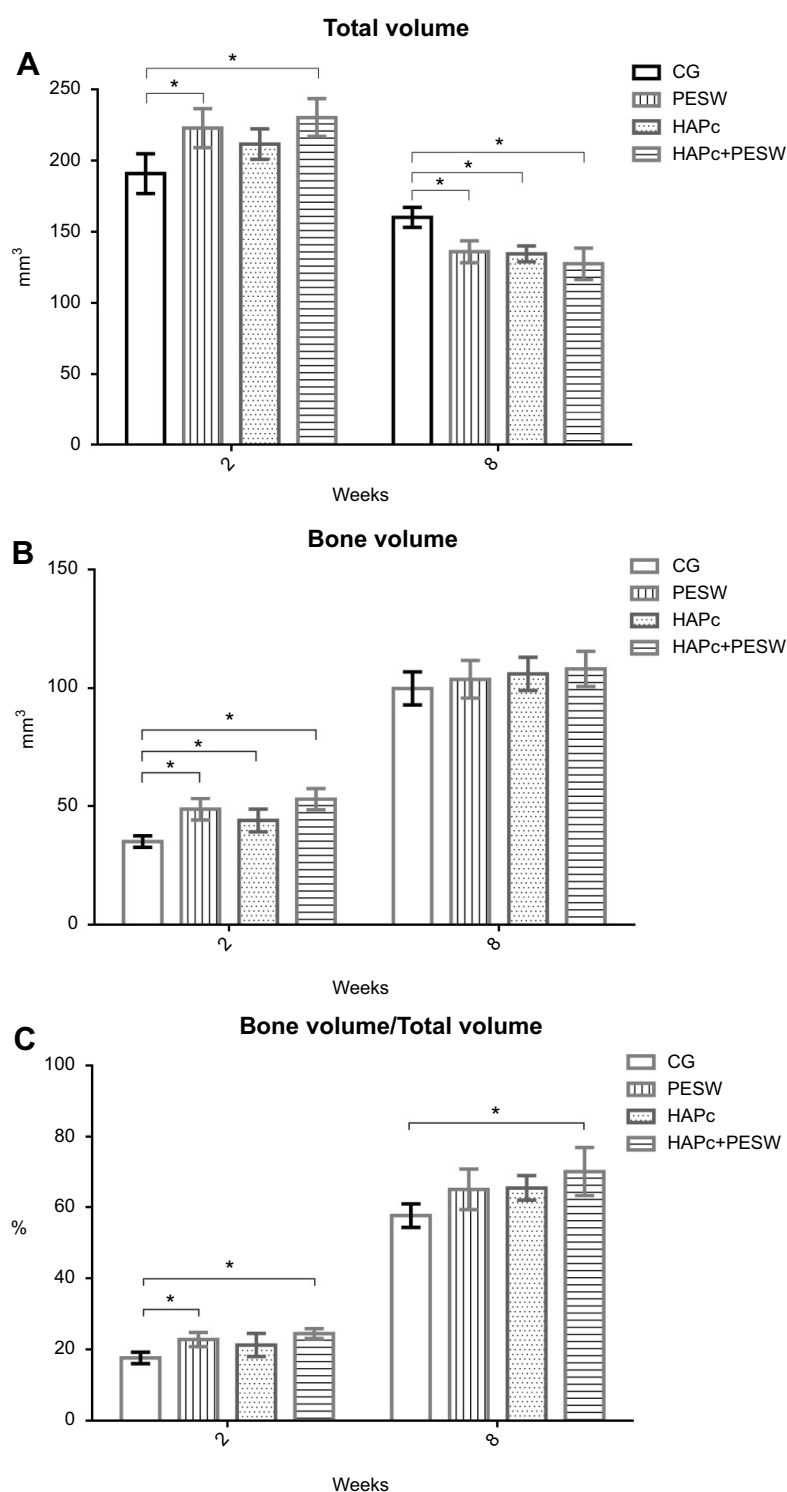
Figure 4 Quantitative analysis of bone microstructure by micro-CT: total tissue volume (TV, **A**), bone volume (BV, **B**) and BV/TV ratio (**C**) in the region of interests of the fracture site of rats in CG, and in PESW, HAPc and HAPc+PESW groups at 2 and 8 weeks; significant differences for $P<0.05$ are (*) marked.
Abbreviations: CG = control group; PESW = pulsed electromagnetic short-waves; HAPc = titanium implants coated with multisubstituted hydroxyapatite and collagen; HAPc+PESW = titanium implants coated with multisubstituted hydroxyapatite and collagen and pulsed electromagnetic short-waves.

approximately 75% for ALP (Figure 3A) and about 100% for OCN (Figure 3B). In the CG, there were significantly lower values compared to the other groups due to a less

intense fracture healing process, in the early phase. Furthermore, the ALP and OCN concentrations were slightly higher for the HAPc+PESW group compared to
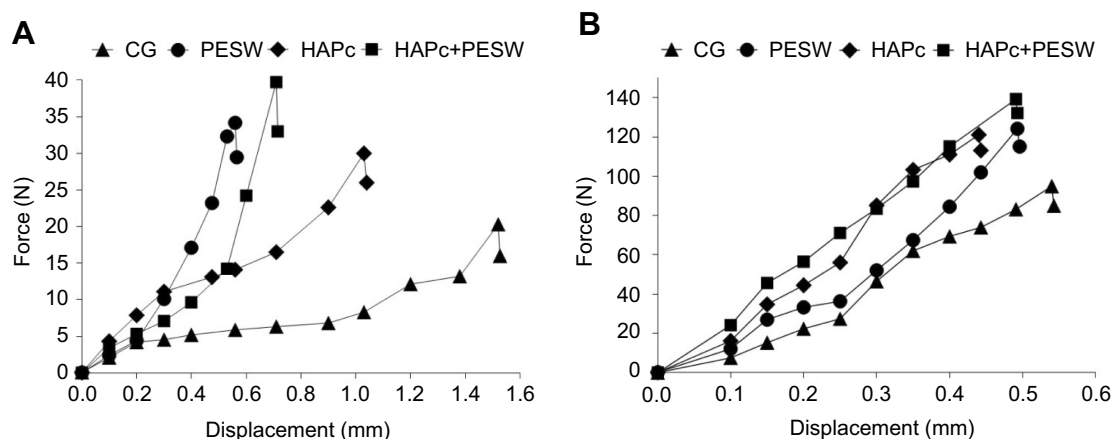
Figure 5 Force vs displacement curves for the three points bending tests performed on the explanted femur of rats: (**A**) at 2 weeks post-implantation and (**B**) at 8 weeks post-implantation.

Abbreviations: CG = control group; PESW = pulsed electromagnetic short-waves; HAPc = titanium implants coated with multisubstituted hydroxyapatite and collagen; HAPc+PESW = titanium implants coated with multisubstituted hydroxyapatite and collagen and pulsed electromagnetic short-waves; N = newton; mm = milimeter.

Table 1 Measured values of the breaking force and the corresponding displacement during the three points bending tests

Group		CG	PESW	HAPc	HAPc+PESW
Ultimate force [N]	2 weeks	20±5	34±4	30±4	40±5
	8 weeks	95±9	124±6	121±8	139±8
Ultimate displacement [mm]	2 weeks	1.5±0.3	0.6±0.2	1.0±0.3	0.7±0.1
	8 weeks	0.6±0.1	0.5±0.1	0.5±0.2	0.5±0.1

Abbreviations: CG = control group; PESW = pulsed electromagnetic short-waves; HAPc = titanium implants coated with multisubstituted hydroxyapatite and collagen; HAPc+PESW = titanium implants coated with multisubstituted hydroxyapatite and collagen and pulsed electromagnetic short-waves; N = newton; mm = milimeter.

the PESW and HAPc groups, but without statistical significance, whereas for PESW and HAPc groups, the values were approximately equal. These findings emphasize that at 2 weeks, due to the exposure to HF-PESW and using the intramedullary fixation with Ti implants (nails) coated by multi-functional ms-HAP/COL@PLA/COL biomimetic composite, there are more osteoblasts that produce ALP and OCN, in HF-PESW, HAPc and PESW groups and thus, a more intense fracture healing process could take place in the early phase of bone consolidation. At 8 weeks, the values decreased in all groups, suggesting a lower bone healing activity in this phase or that the bone consolidation is almost completed.

At 2 weeks post-operative, micro-CT analysis revealed a higher increase in the size of the callus for rats in HAPc+PESW group, exposed to HF-PESW in combination with Ti implants coated with biomimetic HAPc composite (Figure 4A), jointly with PESW group, compared to the CG group. Additionally, a higher BV was found in HAPc+PESW, HAPc and PESW groups (Figure 4B) compared to the CG group. The BV/TV ratios indicated a higher degree of mineralization (Figure 4C) for HAPc+PESW, HAPc and PESW groups compared to the CG group, but without statistical

significance between them. Generally, these findings demonstrated that at 2 weeks there is an advanced fracture healing process, especially in the HAPc+PESW group. Between weeks two and eight, there is a decrease of the TV, which remains significantly higher in the CG compared to the other groups (Figure 4A), while the BV (Figure 4B) and BV/TV ratio (Figure 4C) increase. At 8 weeks post-operative, the BV/TV ratio was significantly higher only for the HAPc+PESW group compared to CG (Figure 4C). Interestingly, the increase in the BV/TV ratio for HAPc+PESW group compared to CG level represents the effect of combined HAPc and PESW method and this effect was found slightly greater than the sum of individual effects. Thus, by using the combined method, namely Ti coated with HAPc composite and HF-PESW stimulation, a positive effect was revealed at 2 and 8 weeks in the HAPc+PESW group.

Our data found at 2 weeks, after the end of the diapulse exposure, evidenced that total TV, BV, and the BV/TV ratio in ROI were higher in HAPc+PESW and PESW groups exposed to HF-PESW, compared to the other groups, with statistical significance for TV, BV and BV/TV ratio compared to CG (Figure 4). Furthermore at 2 weeks, HAPc group showed a significant increase in BV

compared to CG (Figure 4B) and revealed rather equal BV/TV value jointly with PESW group (Figure 4C).

During the mechanical testing, all specimens have shown a continuous increase of the displacement with the force, up to the final failure moment (Figure 5). Thus, the ultimate force can be considered as a good indicator of the strength (Table 1) in the focal point of the fracture. An accurate calculation of the ultimate strength is rather impossible, since the cross-section of the specimens in the focal points is not identical. Nevertheless, the measured values of the ultimate force are different enough between the four categories of specimens and the two time-points, so these can be employed as indicators of the strength in the healed fracture zone.

As it can be seen for all specimens, the measured breaking forces were far higher at 8 weeks, Figure 5B, compared to week 2, Figure 5A (close to 4 times for each case). As expected, CG specimens have shown the smallest strength. HAPc and PESW specimens are quite close in terms of strength, although it can already be stated that HF-PESW treatment assures an increase. It is obvious that the HAPc+PESW specimens displayed the highest strength, both after 2 weeks and after 8 weeks.

In what concerns the ultimate displacement, the specimens harvested after 8 weeks post-implantation show close values (Table 1), while the curves are close to linear, as a result of elastic deformation up to the failure (Figure 5B). This is a typical brittle behavior generated by a complete healing of fractures, in all cases. After 2 weeks, the ultimate displacement values are very dependent upon the type of specimen (Figure 5A). For the groups that were treated with HF-PESW, the ultimate displacement was very similar to the one after 8 weeks, indicating a complete mineralization of the healing callus. This is not the case for HAPc group and CG, where the displacement was far higher, Figure 5A, particularly for CG, while the curves have shown inflexion points, typical for the deformation of complex systems consisting of materials with different stiffness (different Young's moduli). This is in accord with stating that the healing callus is in its soft state for these specimens, predominantly for CG, after 2 weeks.

Analysis of mechanical testing results (Figure 5A) at 2 weeks revealed that HAPc group had higher values of bending strength compared to the CG, and comparable values with PESW group (Table 1). From the four groups, the highest value of bending strength was recorded for HAPc+PESW group, indicating a synergistic effect of the two approaches jointly used. In contrast, at 8 weeks

(Figure 5B), the results obtained in HAPc group were comparable to those of HAPc+PESW and PESW groups exposed to HF-PESW stimulation.

The histological images at 2 weeks showed the persistence of post-fracture hematoma and inflammatory exudation (Figure 6A) in the CG, while in the other groups a soft callus area was identified, which is well defined by the presence of grouped chondrocytes and COL fibers with complete resorption of post-traumatic hematoma (Figures 6B–D). These findings are more evident in HAPc (Figure 6C) and HAPc +PESW (Figure 6D) groups and confirm that the rats treated with Ti implants coated with porous biomimetic HAPc composite and exposed to HF-PESW stimulation have a more advanced stage of bone consolidation, especially when these two methods are jointly used.

Furthermore, the histological images at 8 weeks (Figure 7) revealed in the CG the persistence of small areas of residual cartilage and newly formed spongy bone trabeculae that replaced the soft callus (Figure 7A), while in the group exposed to HF-PESW stimulation the fibro-cartilaginous tissue is completely resorbed and replaced with trabeculae of spongy bone (Figure 7B). Moreover, in the HAPc group, a clear network of trabeculae of bone can be seen with large areas of lamellar bone deposition (Figure 7C). Additionally, in the HAPc+PESW group, the newly formed bone is replaced by lamellar bone and Haversian canals, with a smooth aspect of medullary cavity (Figure 7D), indicating a more advanced stage of bone remodeling.

This study also assessed the in vivo performance of designed Ti implants, in the absence and the presence of HF-PESW stimulation. The ALP and OCN data are relevant only at 2 weeks, as 0 and 8 weeks are outside the maximum activity period. The BV/TV ratios (considered as an indicator of bone mineralization), three points bending test results and histological images are relevant for both time intervals: 2 and 8 weeks.

The CG expressed the most unsatisfying results: the lowest ALP and OCN at 2 weeks; the lower BV/TV ratio at both 2 and 8 weeks; the lowest bending strength in the fracture focal point at both 2 and 8 weeks. In this latter case, the displacement during the test was the highest at both time intervals, proving that the mineralization was not complete and the callus was still in its soft state, in substantial agreement with histological analysis.

The HAPc+PESW group has shown superior results: higher ALP and OCN concentrations at 2 weeks vs CG;
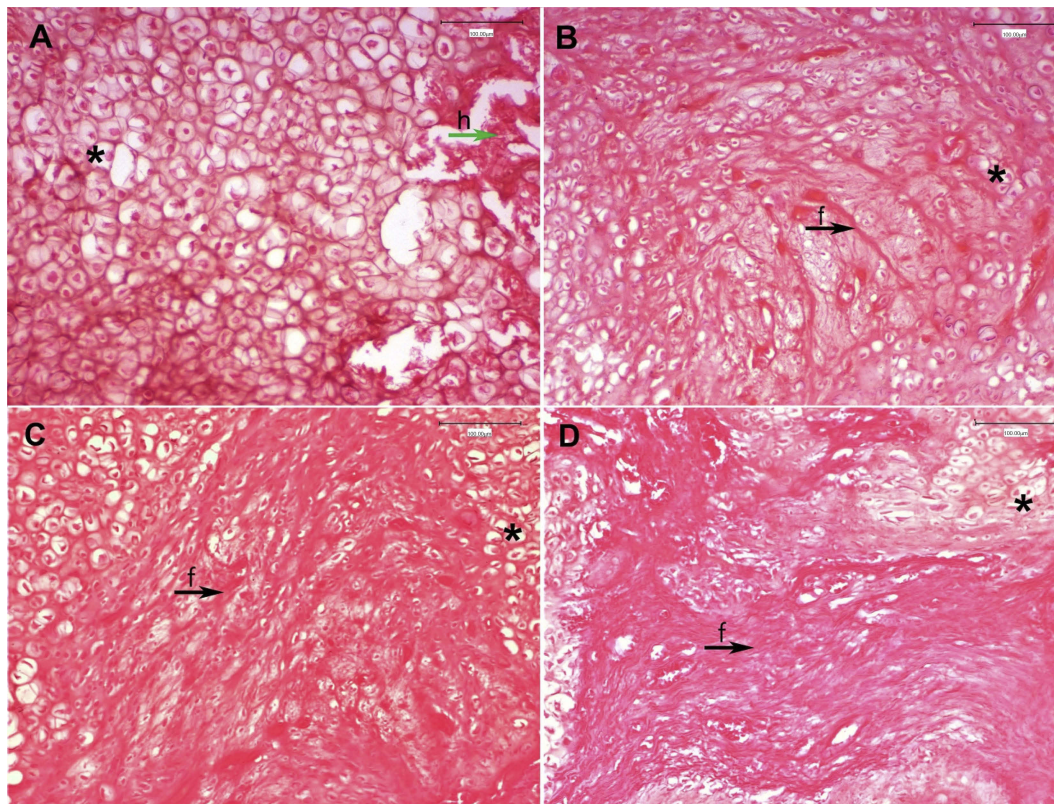
Figure 6 H&E stained at 2 weeks post-surgery, 20× magnification: (**A**) Control group: persistence of post-fracture hematoma (h) and inflammatory exudation at fracture site (h-green arrow), and numerous large chondrocytes (*), without occurrence of newly synthesized collagen fibers; (**B**) PESW group: granulation tissue formation with slight inflammatory infiltrate, small chondrocytes gathered in minor clusters (*) and small amount of individual collagen fibers (f-black arrow) among chondrocytes; (**C**) HAPc group: complete resorption of post-traumatic hematoma and soft callus area formation is well defined by small clusters of grouped chondrocytes (*) separated by well-defined bundle of collagen fibers (f-black arrow) with irregular distribution among chondrocytes; (**D**) HAPc+PESW group: small islands of grouped chondrocytes (*) and the most advanced stage in synthesis of collagen fibers, assembled in dense, regular, abundant collagen bundles (f-black arrow), as a support for the future bone matrix.
Abbreviations: H&E = hematoxylin and eosin; CG = control group; PESW = pulsed electromagnetic short-waves; HAPc = titanium implants coated with multisubstituted hydroxyapatite and collagen; HAPc+PESW = titanium implants coated with multisubstituted hydroxyapatite and collagen and pulsed electromagnetic short-waves.

higher BV/TV values, jointly with PESW group at 2 weeks, and higher absolute at 8 weeks vs CG; the highest bending strength in the fracture site, for both 2 and 8 weeks; complete mineralization and bone fracture healing at 8 weeks in total agreement with histological analysis.

The HAPc and PESW groups were with almost equal values for ALP and OCN, at 2 weeks, and for BV/TV ratios, at 2 and 8 weeks, and have proven better results than CG, but somewhat inferior to HAPc+PESW group.

Specifically, the HAPc group is in vivo more efficient than CG, as clearly demonstrated by BV values shown at 2 weeks, in Figure 4B, for HAPc group>CG (P<0.05). This result emphasizes the importance of the surface treatment of Ti implants. Both types of designed Ti implant surfaces were different in terms of surface roughness, namely uncoated implants owned low surface roughness and HAPc coated implants possessed high-surface roughness, the surface chemical composition, and also the surface morphology. These parameters appear to be essential in the osseointegration process of implants in the host bone and can also strongly intervene in the bone fracture healing, as illustrated in (Figures 6C and 7C, compared to Figures 6A and 7A). This result indicates that a high-surface roughness and the presence of self-assembled COL layer, jointly with ms-HAP/COL NPs distributed in PLA matrix, are critical elements for adhesion, spreading and proliferation of cells on HAPc coated Ti implant surface, and in consequence, for the in vivo effectiveness of the HAPc coated Ti implants. Undoubtedly, pulsing was found to add a positive effect to HAPc coating on Ti implants, as evidenced in the HAPc+PESW group, but only pulsing applied to uncoated Ti implants (PESW group) was not effective enough.

We tried to evidence the osseointegration of designed implants performing a clinical mobility test on living animals and found that the implants were stable. The clinical stability was jointly tested along with bone markers determination, micro-CT results, mechanical tests and histological images.
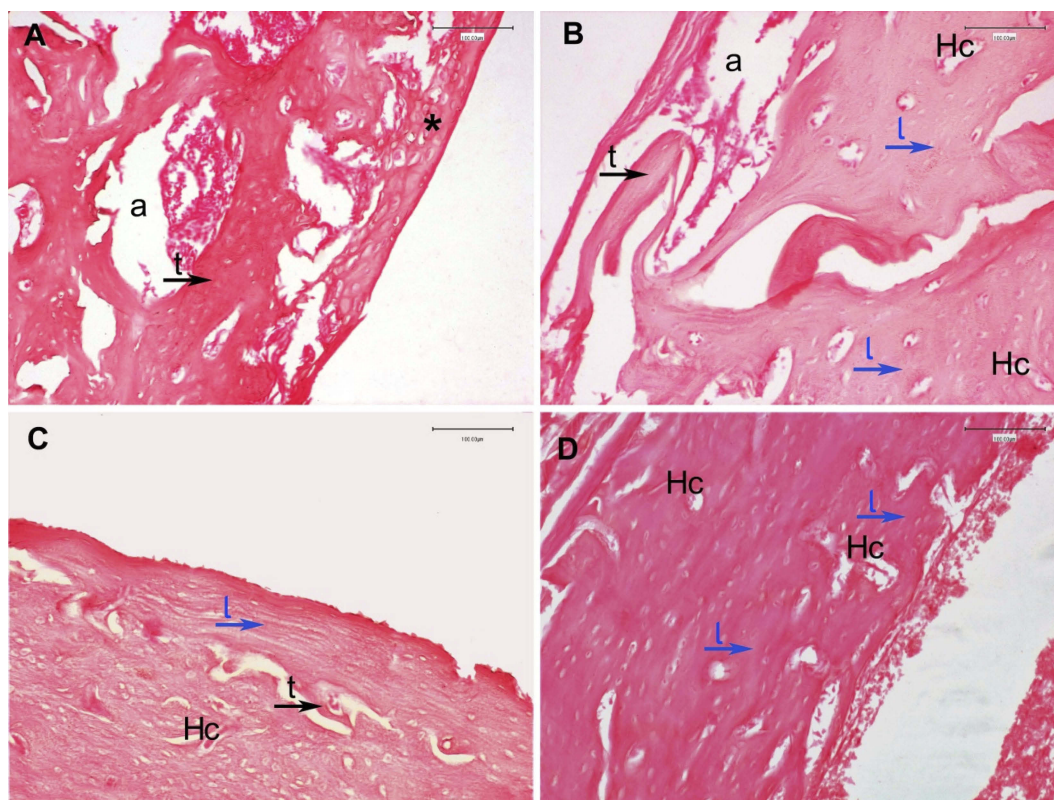
Figure 7 H&E stained at 8 weeks post-surgery, 20× magnification; fracture site at the level of bone–implant interface: (**A**) Control group: incomplete newly formed spongy bone trabeculae (t-black arrow) delimiting areole (a) with bone marrow, and fibro-cartilaginous callus (*), clotted blood formed by inflammation, exudation and residual chondrocytes, partially still present at the fracture level; (**B**) PESW group: fibro-cartilaginous callus is completely resorbed, and a mixture of spongy bone, well-defined trabeculae (t-black arrow) delimiting areole (a), and compact bone (lamellar bone (l-blue arrows) around Haversian canals (Hc)); (**C**) HAPc group: there are less spongy bone trabeculae (t-black arrow), mainly areas of compact lamellar bone deposition (l-blue arrow), and Haversian canals (Hc) with a slightly irregular disposition of bone lamellae around them; (**D**) HAPc+PESW group: newly formed bone is compact lamellar bone (l) with regular, concentric disposition of bone lamellae (l-blue arrows) around Haversian canals (Hc), without areas of spongy bone trabeculae, indicating the more advanced stage of bone remodeling and the most complete bone fracture healing at this phase.
Abbreviations: H&E = hematoxylin and eosin; CG = control group; PESW = pulsed electromagnetic short-waves; HAPc = titanium implants coated with multisubstituted hydroxyapatite and collagen; HAPc+PESW = titanium implants coated with multisubstituted hydroxyapatite and collagen and pulsed electromagnetic short-waves.

These results were evaluated and noticeably indicate the bone fracture healing and bone consolidation. The histological images showed a clear evidence of osseointegration of HAPc coated Ti implants used alone (Figure 7C) or jointly with HF-PESW stimulation (Figure 7D), indicating a more advanced bone remodeling, particularly in the HAPc+PESW group, in substantial agreement with mechanical test results. Additionally, the bonding abilities of biomimetic HAPc composite to natural bone make it a very suitable coating on the surface of metallic implants, ensuring a potential superior effect on their osseointegration.

To the best of our knowledge, the present study on bone fracture healing is the first to investigate the effect of Ti implants coated with HAPc composite in the absence (HAPc group) and in the presence of HF-PESW stimulation (HAPc+PESW group). Therefore, we are unable to compare our results with findings from the literature.

However, consistent to our findings are the studies on the bone response to the fracture, which begins with an inflammatory process and the fracture hematoma[44] with the appearance of pro-inflammatory cytokines and mesenchymal stem cells at this level.[45] Rapid proliferation of these cells leads to the formation of a soft or primary callus that occurs within the first 2 weeks after the trauma.[46] The degree of organization and size of the callus is directly proportional to the cellular activity at the fracture site.[2] Pulsed electromagnetic field stimulation has an effect on the fracture site similar to mechanical loading.[34]

While callus formation facilitates bone healing, an improper fracture stabilization leads to nonunion.[47] Regarding the orthopedic fixation of fractures, we used intramedullary implants,[48] which have the advantage of ensuring multidirectional stability and mechanical strength, thus allowing endochondral healing.[49] To

stabilize the fracture of the femur, we used titanium implants introduced from the intercondylar fossa, because titanium and its alloys are materials of choice for dental and orthopedic implants due to their high physical and chemical properties and biocompatibility.[50] Exposure of the orthopedic implants from the cadaveric models showed that electromagnetic fields produced by MRI and diathermy treatment did not generate a significant increase in local temperature, with a slight increase in tension but without inducing biological changes.[51] Pulsed electromagnetic field stimulation showed no improvement in the osseointegration of commercially pure titanium dental implants at 21 and 42 days on a rabbit model, in terms of histological and mechanical changes.[52] In contrast, porous titanium implants exposed to pulsed electromagnetic fields proved to be effective in repairing bone defects, promoting bone ingrowth and osseointegration, through the Wnt/β-catenin signaling-associated mechanism.[53,54]

Recently, the metal implant surface modification techniques were proposed in order to increase the osseointegration capacity of titanium implants used in cementless arthroplasty.[55] HAP coatings are rather close to the bone in terms of mineral composition[56] and have the potential of carrying osteoinductive growth factors[57] and osteogenic cells.[58] Moreover, zinc (Zn),[59,60] magnesium (Mg),[61] and silicon (Si)[62] enhanced the cytocompatibility of the HAP coating implants[63] and present a beneficial effect on bone growth, osseointegration and bone healing, enhancing in vivo the bone mineral density.[64]

It is also recognized that the collagen-nanohydroxyapatite (COL-HAP) scaffolds can be used as osteoinductive bone graft substitutes because they have a significantly higher osteogenic capacity and better mechanical strength, which make these biomaterials more biocompatible.[12] In a rat model, with the HAP/COL composite for coating Ti rods placed under the calvarium periosteum, HAP/COL coated Ti rods were completely surrounded by new bone tissue, whereas >50% of HAP coated Ti rods were encapsulated in fibrous tissue.[65] Additionally, HAP/COL coating on titanium enhance bonding between titanium and newly formed bone[66] and can be used for cases requiring a better osseointegration.[67]

Compared to the paste of HAP and COL that can physically disperse and its effect may decrease much faster than desired,[68] the use of titanium coated with calcined HAP-COL provides both mechanical stability and rigidity of the fixing method, maintaining long-term osteoconductive properties.[69] Furthermore, substituted HAP in physiological conditions continuously releases its ions,[70] with specific effects in the bone biochemistry and homeostasis.[71] Also, the use of titanium coated with COL type I/chondroitin sulfate showed a better integration at the bone–implant interface in osteoporosis.[72] Pulsed electromagnetic fields in combination with bone marrow cells on COL scaffolds had a greater effect on osteochondral regeneration than used separately.[73]

Our in vivo study showed that the combination of Ti implants, coated with porous biomimetic ms-HAP/COL@PLA/COL (ie HAPc) composite, and HF-PESW stimulation, for 2 weeks, exhibited a synergistic effect on bone fracture healing and bone consolidation, promoting an accelerated bone formation and improved mineralization. The findings were evaluated by serological determination of ALP and OCN, as well as by micro-CT data, mechanical tests and histological analysis. Results demonstrate that the biomimetic ms-HAP/COL@PLA/COL composite, particularly HAP-1.5%Mg-0.2%Zn-0.2%Si/COL@PLA/COL, has a remarkable osteoconductivity and stimulates osteoblasts to produce efficiently the new healthy bone and assure an enhanced bone consolidation. Thus, using the HF-PESW stimulation jointly with titanium implants coated with biomimetic HAPc composite positively influenced the bone consolidation process in its early phase.

These findings also indicate an innovative approach to enhance the bone consolidation and improve the fracture healing around the Ti implants, minimizing the effect of trauma caused by surgery, as observed by bone development phases. Certainly, this HAPc coating has the ability to bond with the bone tissue and so improves the implant stability and may reduce the healing time after surgery.

Conclusion

Noticeably, this in vivo evaluation has demonstrated that the combination of HF-PESW stimulation with HAPc coating on Ti implants promotes an accelerated healing process of bone fracture, enhancing bone consolidation in its early phase. Consequently, this combined method is potentially interesting for clinical applications, proving a superior approach for surface modification of biomedical implants.

Acknowledgment

Author contributions

Daniel Oltean-Dan (DOD), Gheorghe Tomoaia (GT), Gabriela-Bombonica Dogaru (GBD) and Maria Tomoaia-Cotisel (MTC) conceived the project, designed the experiments and jointly wrote the manuscript. DOD and GBD equally contributed to this article and each deserves to be the principal author. DOD, GT, Horea-Rares-Ciprian Benea (HRCB), Dragos Apostu (DA), Alexandru Mester (AM), Mihai-Gheorghe Paiusan (MGP), Cristian Berce (CB) carried out the animal study and animal surgery. CB carried out micro-CT investigation. Elena-Mihaela Jianu (EMJ) performed the histological analysis. Alina-Mihaela Toader (AMT) and Gyorgy-Istvan Bodizs (GIB) carried out bone markers (ALP and OCN) assessment. Catalin-Ovidiu Popa (COP) achieved mechanical testing. Aurora Mocanu (AM), GT, DOD, Reka Balint (RB) and MTC performed the fabrication and characterization of the biomimetic composites and Ti implants. DOD, GBD and MTC analyzed the data for bone markers and micro-CT. DOD and GBD performed statistical analysis. GT and MTC are corresponding authors. All authors contributed to the data analysis, drafting and revising the manuscript and gave the approval for final version of article to be published. The authors agree to be accountable for all aspects of this study.

Disclosure

The authors report no conflicts of interest in this work.

References

1. Buza JA, Einhorn T. Bone healing in 2016. *Clin Cases Miner Bone Metab*. 2016;13(2):101–105. doi:10.11138/ccmbm/2016.13.2.101
2. Gómez-Barrena E, Rosset P, Lozano D, Stanovici J, Ermthaller C, Gerbhard F. Bone fracture healing: cell therapy in delayed unions and nonunions. *Bone*. 2015;70:93–101. doi:10.1016/j.bone.2014.07.033
3. Dimitriou R, Mataliotakis GI, Angoules AG, Kanakaris NK, Giannoudis PV. Complications following autologous bone graft harvesting from the iliac crest and using the RIA: a systematic review. *Injury*. 2011;42(suppl 2):S3–S15. doi:10.1016/j.injury.2011.06.015
4. Lu JW, Yang F, Ke QF, Xie XT, Guo YP. Magnetic nanoparticles modified-porous scaffolds for bone regeneration and photothermal therapy against tumors. *Nanomedicine*. 2018;14(3):811–822. doi:10.1016/j.nano.2017.12.025
5. Antoniac I, Sinescu C, Antoniac A. Adhesion aspects in biomaterials and medical devices. *J Adhes Sci Technol*. 2016;30(16):1711–1715.
6. Rau JV, Antoniac I, Cama G, Komlev VS, Ravaglioli A. Bioactive materials for bone tissue engineering. *Biomed Res Int*. 2016;2016 (Article ID 3741428):1–3. doi:10.1155/2016/3741428
7. Lyons FG, Gleeson JP, Partap S, Coghlan K, O'Brien FJ. Novel microhydroxyapatite particles in a collagen scaffold: a bioactive bone void filler? *Clin Orthop Relat Res*. 2014;472(4):1318–1328. doi:10.1007/s11999-013-3438-0

8. Degasne I, Baslé MF, Demais V, et al. Effects of roughness, fibronectin and vitronectin on attachment, spreading, and proliferation of human osteoblast-like cells (Saos-2) on titanium surfaces. *Calcif Tissue Int*. 1999;64(6):499–507.
9. Frosch KH, Sondergeld I, Dresing K, et al. Autologous osteoblasts enhance osseointegration of porous titanium implants. *J Orthop Res*. 2003;21(2):213–223. doi:10.1016/S0736-0266(02)00143-2
10. Shahrezaee M, Salehi M, Keshtkari S, Oryan A, Kamali A, Shekarchi B. In vitro and in vivo investigation of PLA/PCL scaffold coated with metformin-loaded gelatin nanocarriers in regeneration of critical-sized bone defects. *Nanomedicine*. 2018;14(7):2061–2073. doi:10.1016/j.nano.2018.06.007
11. Tomoaia G, Pasca RD. On the collagen mineralization. A review. *Clujul Med*. 2015;88(1):15–22. doi:10.15386/cjmed-359
12. Cunniffe GM, Curtin CM, Thompson EM, Dickson GR, O'Brien FJ. Content-dependent osteogenic response of nanohydroxyapatite: an in vitro and in vivo assessment within collagen-based scaffolds. *ACS Appl Mater Interfaces*. 2016;8(36):23477–23488. doi:10.1021/acsami.6b06596
13. Yu F, Li M, Yuan Z, et al. Mechanism research on a bioactive resveratrol–PLA–gelatin porous nano-scaffold in promoting the repair of cartilage defect. *Int J Nanomed*. 2018;13:7845–7858. doi:10.2147/IJN.S181855
14. Tsuchiya A, Sotome S, Asou Y, et al. Effects of pore size and implant volume of porous hydroxyapatite/collagen (HAp/Col) on bone formation in a rabbit bone defect model. *J Med Dent Sci*. 2008;55 (1):91–99.
15. Ibrahim DM, Mostafa AA, Korowash SI. Chemical characterization of some substituted hydroxyapatites. *Chem Cent J*. 2011;5(1):74. doi:10.1186/1752-153X-5-74
16. Tomoaia G, Soritau O, Tomoaia-Cotisel M, et al. Scaffolds made of nanostructured phosphates, collagen and chitosan for cell culture. *Powder Technol*. 2013;238:99–107. doi:10.1016/j.powtec.2012.05.023
17. Tomoaia G, Mocanu A, Vida-Simiti I, et al. Silicon effect on the composition and structure of nanocalcium phosphates: in vitro biocompatibility to human osteoblasts. *Mater Sci Eng C Mater Biol Appl*. 2014;37(1):37–47. doi:10.1016/j.msec.2013.12.027
18. Mocanu A, Furtos G, Rapuntean S, et al. Synthesis; characterization and antimicrobial effects of composites based on multi-substituted hydroxyapatite and silver nanoparticles. *Appl Surf Sci*. 2014;298:225–235. doi:10.1016/j.apsusc.2014.01.166
19. Goga F, Forizs E, Avram A, et al. Synthesis and thermal treatment of hydroxyapatite doped with magnesium, zinc and silicon. *Rev Chim*. 2017;68(6):1193–1200.
20. Goga F, Forizs E, Borodi G, et al. Behavior of doped hydroxyapatites during the heat treatment. *Rev Chim*. 2017;68(12):2907–2913.
21. Ren F, Leng Y, Xin R, Ge X. Synthesis, characterization and ab initio simulation of magnesium-substituted hydroxyapatite. *Acta Biomater*. 2010;6(7):2787–2796. doi:10.1016/j.actbio.2009.12.044
22. Frangopol PT, Mocanu A, Almasan V, et al. Synthesis and structural characterization of strontium substituted hydroxyapatites. *Rev Roum Chim*. 2016;61(4–5):337–344.
23. Izquierdo-Barba I, Santos-Ruiz L, Becerra J, et al. Synergistic effect of Si-hydroxyapatite coating and VEGF adsorption on Ti6Al4V-ELI scaffolds for bone regeneration in an osteoporotic bone environment. *Acta Biomater*. 2019;83:456–466. doi:10.1016/j.actbio.2018.11.017
24. Zhu A, Lu P, Wu H. Immobilization of poly(ε-caprolactone)–poly (ethylene oxide)–poly(ε-caprolactone) triblock copolymer on poly (lactide-co-glycolide) surface and dual biofunctional effects. *Appl Surf Sci*. 2007;253(6):3247–3253. doi:10.1016/j.apsusc.2006.07.036
25. Li J, Lu XL, Zheng YF. Effect of surface modified hydroxyapatite on the tensile property improvement of HA/PLA composite. *Appl Surf Sci*. 2008;255(2):494–497. doi:10.1016/j.apsusc.2008.06.067

26. Hrubovcakova M, Kupkova M, Dzupon M, Giretova M, Medvecky L, Dzunda R. Biodegradable polylactic acid and polylactic acid/hydroxyapatite coated iron foams for bone replacement materials. *Int J Electrochem Sci*. 2017;12(12):11122–11136. doi:10.20964/2017.12.53

27. Yang W, Yin G, Zhou D, Gu J, Li Y, Zhang H. Biocompatibility of surface-modified biphasic calcium phosphate/poly-L-lactide biocomposite in vitro and in vivo. *J Mater Sci Technol*. 2010;26(8):754–758. doi:10.1016/S1005-0302(10)60119-3

28. Vashisth P, Bellare JR. Development of hybrid scaffold with biomimetic 3D architecture for bone regeneration. *Nanomedicine*. 2018;14 (4):1325–1336. doi:10.1016/j.nano.2018.03.011

29. Tomoaia G, Pop LB, Petean I, Tomoaia-Cotisel M. Significance of surface structure on orthopedic materials. *Mater Plast*. 2012;49(1):48–54.

30. Shapovalova Y, Lytkina D, Rasskazova L, et al. P97: bioresorbable composites based on hydroxyapatite dispersed in poly-L-lactide matrix. *Eur J Cancer Suppl*. 2015;13(1):49–50. doi:10.1016/j. ejcsup.2015.08.088

31. Kubasiewicz-Ross P, Hadzik J, Seeliger J, et al. New nano-hydroxyapatite in bone defect regeneration: a histological study in rats. *Ann Anat*. 2017;213:83–90. doi:10.1016/j.aanat.2017.05.010

32. Tomoaia G, Tomoaia-Cotisel M, Pop LB, et al. Synthesis and characterization of some composites based on nanostructured phosphates, collagen and chitosan. *Rev Roum Chim*. 2011;56(10–11):1039–1046.

33. Russias J, Saiz E, Nalla RK, Gryn K, Ritchie RO, Tomsia AP. Fabrication and mechanical properties of PLA/HA composites: a study of in vitro degradation. *Mater Sci Eng C Biomim Supramol Syst*. 2006;26(8):1289–1295. doi:10.1016/j.msec.2005.08.004

34. Galkowski V, Brad P, Drew B, Dick D. Bone stimulation for fracture healing: what′s all the fuss? *Indian J Orthop*. 2009;43(2):117–120. doi:10.4103/0019-5413.50844

35. Taylor KF, Inoue N, Rafiee B, Tis JE, McHale KA, Chao EY. Effect of pulsed electromagnetic fields on maturation of regenerate bone in a rabbit limb lengthening model. *J Orthop Res*. 2006;24(1):2–10. doi:10.1002/jor.20014

36. Hannemann PF, Mommers EH, Schots JP, Brink PR, Poeze M. The effects of low-intensity pulsed ultrasound and pulsed electromagnetic fields bone growth stimulation in acute fractures: a systematic review and meta-analysis of randomized controlled trials. *Arch Orthop Trauma Surg*. 2014;134(8):1093–1106. doi:10.1007/s00402-014-2014-8

37. Tsai MT, Li WJ, Tuan RS, Chang WH. Modulation of osteogenesis in human mesenchymal stem cells by specific pulsed electromagnetic field stimulation. *J Orthop Res*. 2009;27(9):1169–1174. doi:10.1002/ jor.20862

38. Chang K, Chang WH, Huang S, Huang S, Shih C. Pulsed electromagnetic fields stimulation affects osteoclast formation by modulation of osteoprotegerin, RANK ligand and macrophage colony-stimulating factor. *J Orthop Res*. 2005;23(6):1308–1314. doi:10.1016/j.orthres. 2005.03.012.1100230611

39. Teven CM, Greives M, Natale RB, et al. Differentiation of osteoprogenitor cells is induced by high-frequency pulsed electromagnetic fields. *J Craniofac Surg*. 2012;23(2):586–593. doi:10.1097/ SCS.0b013e31824cd6de

40. Park JW, Kim YJ, Jang JH, Kwon TG, Bae YC, Suh JY. Effects of phosphoric acid treatment of titanium surfaces on surface properties, osteoblast response and removal of torque forces. *Acta Biomater*. 2010;6(4):1661–1670. doi:10.1016/j.actbio.2009.10.011

41. Tomoaia G, Tomoaia-Cotisel M, Mocanu A, et al. Supramolecular organization of collagen and anti-cancer drugs. *J Optoelectron Adv Mater*. 2008;10(4):961–964.

42. Mocanu A, Pasca RD, Tomoaia G, et al. New procedure to synthesize silver nanoparticles and their interaction with local anesthetics. *Int J Nanomedicine*. 2013;8:3867–3874. doi:10.2147/IJN.S51063

43. Rau JV, Fosca M, Cacciotti I, Laureti S, Bianco A, Teghil R. Nanostructured Si-substituted hydroxyapatite coatings for biomedical applications. *Thin Solid Films*. 2013;543:167–170. doi:10.1016/j. tsf.2012.12.113

44. Loi F, Cordova LA, Pajarinen J, Lin TH, Yao Z, Goodman SB. Inflammation, fracture and bone repair. *Bone*. 2016;86:119–130. doi:10.1016/j.bone.2016.02.020

45. Lin W, Xu L, Zwingenberger S, et al. Mesenchymal stem cells homing to improve bone healing. *J Orthop Transl*. 2017;9:19–27.

46. Mirhadi S, Ashwood N, Karagkevrekis B. Factors influencing fracture healing. *Trauma*. 2013;15(2):140–155. doi:10.1177/1460408613486571

47. Marsh DR, Li G. The biology of fracture healing: optimising outcome. *Br Med Bull*. 1999;55(4):856–869. doi:10.1258/0007142991902673

48. Klymov A, Te Riet J, Mulder P, Gardeniers JGE, Jansen JA, Walboomers XF. Nanometer-grooved topography stimulates trabecular bone regeneration around a concave implant in a rat femoral medulla model. *Nanomedicine*. 2016;12(8):2283–2290. doi:10.1016/ j.nano.2016.06.013

49. Wehner T, Claes L, Ignatius A, Simon U. Optimization of intramedullary nailing by numerical simulation of fracture healing. *J Orthop Res*. 2012;30(4):569–573. doi:10.1002/jor.21568

50. Goutam M, Giriyapura C, Mishra SK, Gupta S. Titanium allergy: a literature review. *Indian J Dermatol*. 2014;59(6):630. doi:10.4103/ 0019-5154.143526

51. Crouzier D, Selek L, Martz BA, Dabouis V, Arnaud R, Debouzy JC. Risk assessment of electromagnetic fields exposure with metallic orthopedic implants: a cadaveric study. *Orthop Traumatol Surg Res*. 2012;98(1):90–96. doi:10.1016/j.otsr.2011.08.012

52. Buzza EP, Shibli JA, Barbeiro RH, Barbosa JR. Effects of electromagnetic field on bone healing around commercially pure titanium surface: histologic and mechanical study in rabbits. *Implant Dent*. 2003;12(2):182–187.

53. Jing D, Zhai M, Tong S, et al. Pulsed electromagnetic fields promote osteogenesis and osseointegration of porous titanium implants in bone defect repair through a Wnt/β-catenin signaling-associated mechanism. *Sci Rep*. 2016;6(1):32045. doi:10.1038/srep32045

54. Zhang Z, Li Z, Zhang C, et al. Biomimetic intrafibrillar mineralized collagen promotes bone regeneration via activation of the Wnt signaling pathway. *Int J Nanomed*. 2018;13:7503–7516. doi:10.2147/IJN.S172164

55. Sirin HT, Vargel I, Kutsal T, Korkusuz P, Piskin E. Ti implants with nanostructured and HA-coated surfaces for improved osseointegration. *Artif Cells Nanomed Biotechnol*. 2016;44(3):1023–1030. doi:10.3109/21691401.2015.1008512

56. Lin X, Yang S, Lai K, Yang H, Webster TJ, Yang L. Orthopedic implant biomaterials with both osteogenic and anti-infection capacities and associated in vivo evaluation methods. *Nanomedicine*. 2017;13(1):123–142. doi:10.1016/j.nano.2016.08.003

57. Attia N, Mashal M, Grijalvo S, et al. Stem cell-based gene delivery mediated by cationic niosomes for bone regeneration. *Nanomedicine*. 2018;14(2):521–531. doi:10.1016/j.nano.2017.11.005

58. Henkel J, Woodruff MA, Epari DR, et al. Bone regeneration based on tissue engineering conceptions – a 21st century perspective. *Bone Res*. 2013;1(3):216–248. doi:10.4248/BR201303002

59. Ding Q, Zhang X, Huang Y, Yan Y, Pang X. In vitro cytocompatibility and corrosion resistance of zinc-doped hydroxyapatite coatings on a titanium substrate. *J Mater Sci*. 2015;50(1):189–202. doi:10.1007/s10853-014-8578-4

60. Garbo C, Sindilaru M, Carlea A, et al. Synthesis and structural characterization of novel porous zinc substituted nanohydroxyapatite powders. *Part Sci Technol*. 2017;35(1):29–37. doi:10.1080/02726351.2015.1121180

61. Cai YL, Zhang J, Zhang S, et al. Osteoblastic cell response on fluoridated hydroxyapatite coatings: the effect of magnesium incorporation. *Biomed Mater*. 2010;5(5):054114. doi:10.1088/1748-6041/5/3/035008

62. Thian ES, Huang J, Best SM, Barber ZH, Bonfield W. Novel silicon-doped hydroxyapatite (Si-HA) for biomedical coatings: an in vitro study using a cellular simulated body fluid. *J Biomed Mater Res B Appl Biomater*. 2006;76B(2):326–333. doi:10.1002/jbm.b.30368

63. Macha IJ, Ben-Nissan B, Santos J, et al. Biocompatibility of a new biodegradable polymer-hydroxyapatite composite for biomedical applications. *J Drug Deliv Sci Technol*. 2017;38:72–77. doi:10.1016/j. jddst.2017.01.008

64. Beck GR, Ha SW, Camalier CE, et al. Bioactive silica-based nano-particles stimulate bone-forming osteoblasts, suppress bone-resorbing osteoclasts, and enhance bone mineral density in vivo. *Nanomedicine*. 2012;8(6):793–803. doi:10.1016/j.nano.2011.11.003

65. Uezono M, Takakuda K, Kikuchi M, Suzuki S, Moriyama K. Hydroxyapatite/collagen nanocomposite-coated titanium rod for achieving rapid osseointegration onto bone surface. *J Biomed Mater Res B Appl Biomater*. 2013;101B(6):1031–1038. doi:10.1002/jbm.b.32913

66. Murakami A, Arimoto T, Suzuki D, et al. Antimicrobial and osteogenic properties of a hydrophilic-modified nanoscale hydroxyapatite coating on titanium. *Nanomedicine*. 2012;8(3):374–382. doi:10.1016/j.nano.2011.07.001

67. Itoh S, Kikuchi M, Koyama Y, et al. Development of a novel biomaterial, hydroxyapatite/collagen (HAp/Col) composite for medical use. *Biomed Mater Eng*. 2005;15(1–2):29–41.

68. Wei X, Egawa S, Matsumoto R, et al. Augmentation of fracture healing by hydroxyapatite/collagen paste and bone morphogenetic protein-2 evaluated using a rat femur osteotomy model. *J Orthop Res*. 2018;36(1):129–137. doi:10.1002/jor.23646

69. Walmsley GG, McArdle A, Tevlin R, et al. Nanotechnology in bone tissue engineering. *Nanomedicine*. 2015;11(5):1253–1263. doi:10.1016/j.nano.2015.02.013

70. Sprio S, Tampieri A, Landi E, et al. Physico-chemical properties and solubility behaviour of multi-substituted hydroxyapatite powders containing silicon. *Mater Sci Eng C*. 2008;28(1):179–187. doi:10.1016/j.msec.2006.11.009

71. Govindaraj D, Rajan M, Munusamy MA, Alarfai AA, Sadasivuni KK, Kumar SS. The synthesis, characterization and in vivo study of mineral substituted hydroxyapatite for prospective bone tissue rejuvenation applications. *Nanomedicine*. 2017;13(8):2661–2669. doi:10.1016/j.nano.2017.07.017

72. Kyllönen L, D'Este M, Alini M, Eglin D. Local drug delivery for enhancing fracture healing in osteoporotic bone. *Acta Biomater*. 2015;11(1):412–434. doi:10.1016/j.actbio.2014.09.006

73. Veronesi F, Cadossi M, Giavaresi G, et al. Pulsed electromagnetic fields combined with a collagenous scaffold and bone marrow concentrate enhance osteochondral regeneration: an in vivo study. *BMC Musculoskelet Disord*. 2015;16(1):233.